Geophys. J. Int. (2001) **146,** 399–415

Classification of seismic strain estimates in the Mediterranean region from a 'bootstrap' approach

Marcello Viti, Dario Albarello and Enzo Mantovani

Department of Earth Sciences, University of Siena, Via Laterina 8, 53100 *Siena, Italy. E-mail: vitimar@unisi.it*

Accepted 2001 March 16. Received 2001 March 16; in original form 2000 August 10

SUMMARY

The uncertainty that may affect seismic strain estimates in the Mediterranean is investigated using a distribution-free numerical approach based on the bootstrap resampling technique, applied to more than 2000 seismic source mechanisms of shallow earthquakes that occurred from the Azores to Iran in the period 1905–1999. This analysis shows that the short time interval covered by the available data set may be the main source of uncertainty on long-term strain estimates, since it could imply a biased representation of contributions from large earthquakes. Our results also indicate that, as a possible consequence of this bias, the condition of strain field uniformity is poorly verified in most of the zones considered. The confidence limits obtained for scalar strains and directions of principal strain axes indicate that both the amount and the style of seismic deformation are poorly defined for roughly half of the zones considered, mostly located in the western and central Mediterranean area. These results suggest that one should be cautious in using seismic strain estimates when not accompanied by satisfactorily uncertainty evaluation.

Key words: crustal deformation, fault plane solutions, Mediterranean region, regionalization, seismotectonics.

INTRODUCTION

The Mediterranean area is widely recognized as the collision zone between the African, Arabian and Eurasian plates. The deformation pattern caused by the convergence of these plates is characterized by a complex space–time distribution of compressional and tensional events, with the opening of relatively large basins such as the Balearic, Tyrrhenian, Pannonian and Aegean (Fig. 1), and the strong distortion, with lateral migrations of several hundred kilometres, of Palaeogene–Neogene orogenic belts (e.g. Dercourt *et al*. 1986). As a final result of this complex evolution, the Mediterranean region at present is comprised of a number of crustal wedges derived from the fragmentation of continental domains and the dissection of orogenic belts (Mantovani *et al*. 1997, 2000a).

The reconstruction of the present kinematic pattern of such a plate/microplate mosaic may be carried out by space geodesy techniques (GPS, VLBI, SLR) or by the analysis of geological and seismological strain indicators. The increasing number of permanent GPS stations all over the Mediterranean area suggests that the contribution of this kind of technique to plate motion analysis will become increasingly important (Reilinger *et al*. 1997; Kahle *et al.* 1998, 1999, 2000; McClusky *et al*. 2000). However, a high number of permanent stations would be necessary to resolve the strong lateral variations of deformation style occurring in the entire Mediterranean region. Owing to this problem, geodetic measurements can be taken as reliable constraints on plate kinematics in only a few zones where dense station networks are available. Moreover, in a region of relatively low motion rates, as is the case for most of the area considered here, geodetic surveys should cover an adequately long time interval (some tens of years at least) to provide significant results.

Information about the recent/present kinematic field can also be inferred from neotectonic and seismic data. In particular, an estimate of average seismic strain occurring in active zones can be obtained by summing earthquake moment tensors (Kostrov 1974). This method has been extensively used in the Mediterranean region (Ekström & England 1989; Jackson & McKenzie 1988; Jackson *et al*. 1992; Kiratzi 1991, 1993; Papazachos & Kiratzi 1996; Papazachos *et al*. 1992, 1998; Pondrelli 1999; Pondrelli *et al*. 1995). Since this kind of estimate may provide important constraints for geodynamic modelling (e.g. Sobouti & Arkani-Hamed 1996; Lundgren *et al*. 1998; Mantovani *et al*. 2000b, 2001) and seismic hazard assessment (e.g. Ward 1998), a rigorous evaluation of the uncertainties involved is required.

Estimating long-term seismic strain rates from limited catalogues may involve four major sources of uncertainty. The first derives from the randomness of earthquake occurrence in time and space. A first-order estimate of such uncertainty,

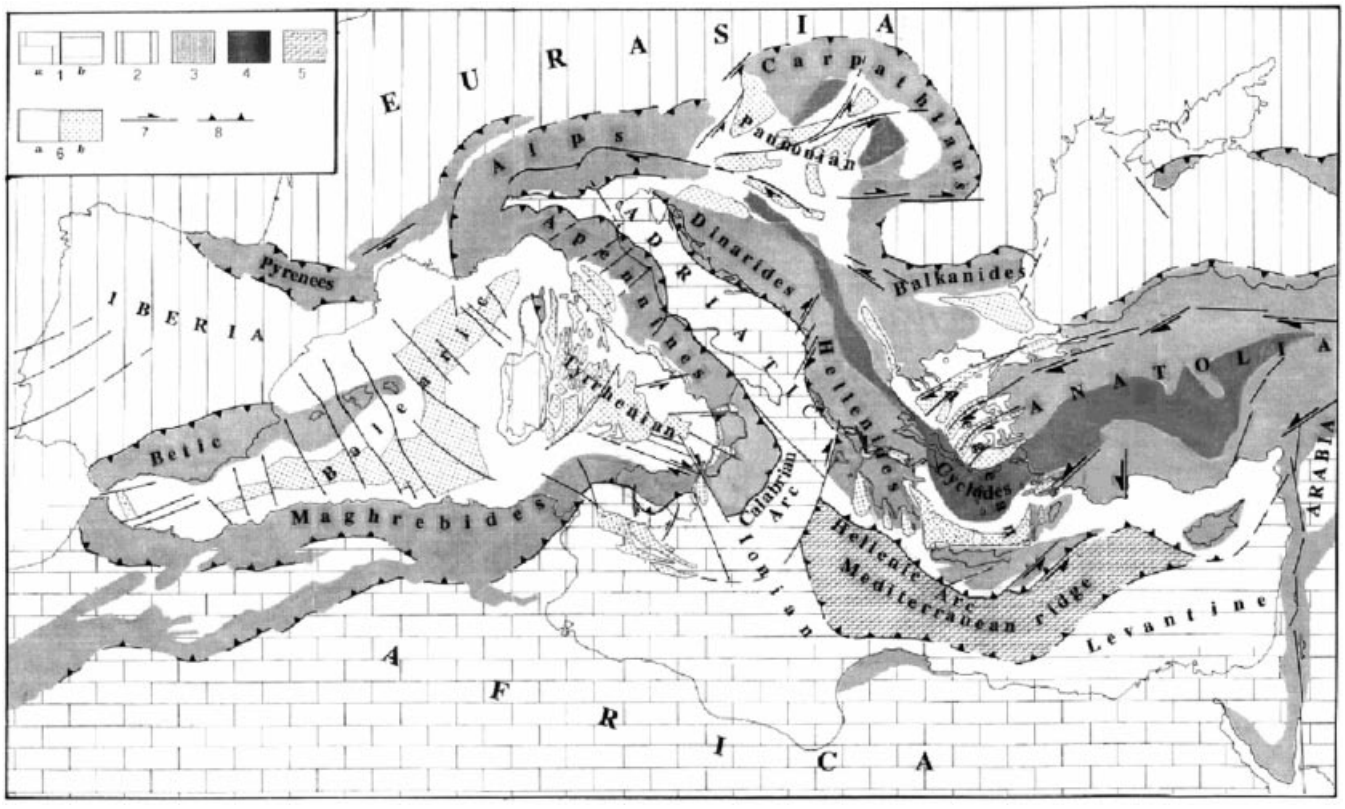

Figure 1. Main morphological and tectonic features of the Mediterranean area. (1) African/Adriatic domain with continental (a) and thinned (b) crust; (2) Eurasian domain; (3) deformation belts; (4) internal massifs of the Tethyan belts; (5) accretionary zone of the Hellenic Arc (Mediterranean ridge); (6) zones affected by moderate (a) or intense (b) crustal thinning since the Oligocene; (7,8) main transforms and compressional features. Details and references on recent/present Mediterranean tectonics and evolutionary history are given by Mantovani *et al.* (1997, 2000a).

under the restrictive condition that earthquake occurrence can be considered as a Poisson random process, has been performed by Shen-Tu *et al.* (1998).

A second source of uncertainty derives from experimental errors on seismic moment tensors. Some authors have proposed evaluating the effect of such an uncertainty by linear propagation of errors affecting fault plane solutions and seismic moments (e.g. Wyss *et al.* 1992; Papazachos & Kiratzi 1992; Shen-Tu *et al.* 1995). However, this approach is relatively rough since it does not take into account the mutual correlation among errors on source parameters and the strong non-linearity of error propagation. In any case, some indirect estimates (Shen-Tu *et al.* 1998) suggest that the contribution of experimental errors may be completely overshadowed by the effect of randomness in the occurrence of earthquakes.

The third source of uncertainty is catalogue incompleteness, which derives from the lack of events that actually occurred during the time span covered by the available catalogue. Obviously, this last problem mainly concerns minor events, a number of which fall below the detectability threshold. In any case, one must be aware that fault plane solutions are available for only a subset of the earthquakes actually recorded in the period considered.

A fourth source of uncertainty is related to the catalogue shortness, which could imply a biased sampling of major events whose return periods exceed the time interval covered by the available data set.

The last two sources do not affect long-term strain estimates deduced from seismic data in the same way since minor earthquakes and larger events contribute in a different way to the overall uncertainty. Some studies (Marrett & Allmendinger 1992; Polimenos 2000) point out the fundamental self-similarity of the fracture process. This phenomenon implies that small earthquakes can contribute significantly to the total amount of strain released. However, the shape of the average strain tensor obtained from small events and that obtained by considering major earthquakes do not show significant differences (Amelung & King 1997). This implies that the lack of information on minor earthquakes may significantly affect the estimate of strain magnitude, but it could not influence the deformation style deduced from major earthquakes only. On the other hand, the same study indicates that an incomplete sampling of the largest events, that is, those characterized by relatively long return periods, can introduce a significant bias in the strain estimate. Indeed, major earthquakes accommodate most of the seismic strain, so that a lack of a major earthquake, due to the small time window considered, could strongly affect the strain estimate. This last source of uncertainty, previously defined as catalogue shortness, cannot easily be evaluated by classical direct approaches. A first-order evaluation of this contribution can be obtained by following an empirical procedure based on distribution-free numerical resampling, i.e. the 'bootstrap' method (e.g. Hall 1992), already applied to seismotectonic studies (e.g. Michael 1987; Shen-Tu *et al.* 1995, 1998; Albarello, 2000). This procedure aims at investigating the population of strain estimates derived from the analysis of a number of new data sets, generated by slightly modifying (randomly) the initial data set. Thus, the effect of the random occurrence (or lack) in

the real data set of low-probability events (i.e. the major ones), which could strongly affect the final estimate, can be tentatively simulated.

This kind of approach could also help to overcome a significant drawback of standard approaches. These presume that the parent population of empirical estimates relative to average strain is essentially unimodal. In this assumption, the sample average and variance derived from available data are taken as sufficient to obtain confidence limits for empirical strain estimates. However, this assumption is realistic only in the case where the strain field in the zone considered is uniform. When complex tectonic zones, such as the Mediterranean one, are under study, this condition and thus the significance of any tectonic interpretation of strain estimates cannot be safely assumed without any preliminary attempt at empirical validation. Bootstrap procedures are essentially distribution-free and thus they do not consider the condition of unimodality. Therefore, these methods may allow one to validate the hypothesis of strain uniformity (associated with the unimodality of the parent population) and to provide a more realistic estimate of uncertainty relative to average strain.

In the present work, the bootstrap procedure has been used to evaluate the reliability of Kostrov's strain estimates in a number of seismic zones of the Mediterranean area.

DATA SET

A catalogue of 2029 focal mechanisms of shallow earthquakes ($h<50$ km) that occurred from September 1905 to March 1999 in the region between 24°N and 53°N and 30°W and 60°E (Fig. 2) has been compiled from the relevant literature (see Appendix A).

Since in most cases the original papers do not report any information about the quality of source mechanisms, a suitable ranking of the level of uncertainty affecting data cannot be performed. Owing to the lack of more justified criteria, the most recent solution has been considered for each earthquake.

The major statistical features of the data set are reported in Fig. 3. The time distribution of earthquakes (Fig. 3a) shows a large data increase after 1980. The distribution of data versus magnitude (Fig. 3b) suggests that the catalogue is largely incomplete only for magnitudes lower than 6. Since most of the earthquakes (84 per cent) are characterized by hypocentral depths of less than 20 km (Fig. 3c), an average thickness of 20 km has been assumed for the seismogenic layer in the whole region considered.

The majority of data (66 per cent) are first-motion source mechanisms. Focal mechanisms obtained by the CMT approach and body waveform inversion represent 23 and 11 per cent, respectively, of the available solutions and are mostly available for the largest earthquakes.

When a CMT solution was not available, moment tensor components were obtained from the fault plane solution and the seismic moment M_0 (Jost & Herrmann 1989). When not reported, the seismic moment was computed using the empirical relationship proposed by Dziewonski & Woodhouse (1983),

$$M_S = 0.668 \log_{10} M_0 - 6.184\,, \tag{1}$$

where M_S is the surface wave magnitude and M_0 is given in N m. Since the relationship between body wave magnitude and seismic moment is characterized by remarkable scatter (Dziewonski & Woodhouse 1983, Fig. 14a), we prefer to convert m_b to M_S using the formula proposed by Kasahara (1981),

$$m_b = 0.63 M_S + 2.5\,, \tag{2}$$

and to use eq.(1) in order to provide an indirect estimate of M_0. This was done only in a few cases where m_b magnitude was the only available measure of earthquake size.

ASSESSMENT AND REPRESENTATION OF STRAIN UNCERTAINTIES

Kostrov's (1974) theorem states that the component ε_{ij} of the average non-rotational strain tensor, related to N earthquakes occurred in a crustal volume V, is given by

$$\varepsilon_{ij} = \frac{\sum_{n=1}^{N} \boldsymbol{M}_{ij}^{(n)}}{2\mu V}\,, \tag{3}$$

where $\boldsymbol{M}_{ij}^{(n)}$ is the seismic moment tensor component of the nth earthquake that occurred in the crustal volume, whose average elastic shear modulus is μ. Eq. (3) provides an incremental strain tensor that is representative of the rate at which the seismic deformation occurs in the crustal volume considered (Twiss & Unruh 1998). The principal values of the strain tensor (eq. 3) are indicated by ε_1, ε_2 and ε_3, respectively, with positive values representing lengthening and $\varepsilon_1 > \varepsilon_2 > \varepsilon_3$. The Euclidean norm, ε_0,

$$\varepsilon = (|\varepsilon_1|^2 + |\varepsilon_2|^2 + |\varepsilon_3|^2)^{1/2}\,, \tag{4}$$

can be used to represent, in the form of a scalar parameter, the amount of average seismic strain accommodated within the crustal volume considered. The principal directions of the average strain tensor (eq. 3) can be used to constrain the shape of the strain ellipsoid and thus the deformation pattern in the zones considered. We tentatively adopt a classification of strain regimes analogous to that used for stress regimes in the analysis of tectonic faulting (Simpson 1997). Since the sum of strain eigenvalues must be zero for a double-couple source (Jost & Herrmann 1989), the vertical eigenvector effectively constrains the strain regime. Thus, we define three canonical strain styles, i.e. 'shortening', 'transform' and 'lengthening', which occur when one of the principal axes is vertical and the related principal value is the maximum (ε_1), intermediate (ε_2) or minimum (ε_3) lengthening, respectively. Crustal thickening, related to the 'shortening' style, is accommodated in the horizontal plane by dominant shortening along one or both principal strain axes. Conversely, crustal thinning, associated with the 'lengthening' style, is accommodated by dominant lengthening along one or both horizontal principal directions. The 'transform' style is related to horizontal shortening and lengthening while the corresponding vertical strain depends on the sign of ε_2.

In order to estimate the uncertainty affecting the strain estimates obtained from eq. (3), a numerical resampling procedure has been adopted. The basic premise of the bootstrap approach (Efron & Tbishirani 1986; Hall 1992) is that the empirical frequency distribution of data provides the maximum likelihood estimate of the probability distribution that characterizes the unknown parent population. This hypothesis implies that new

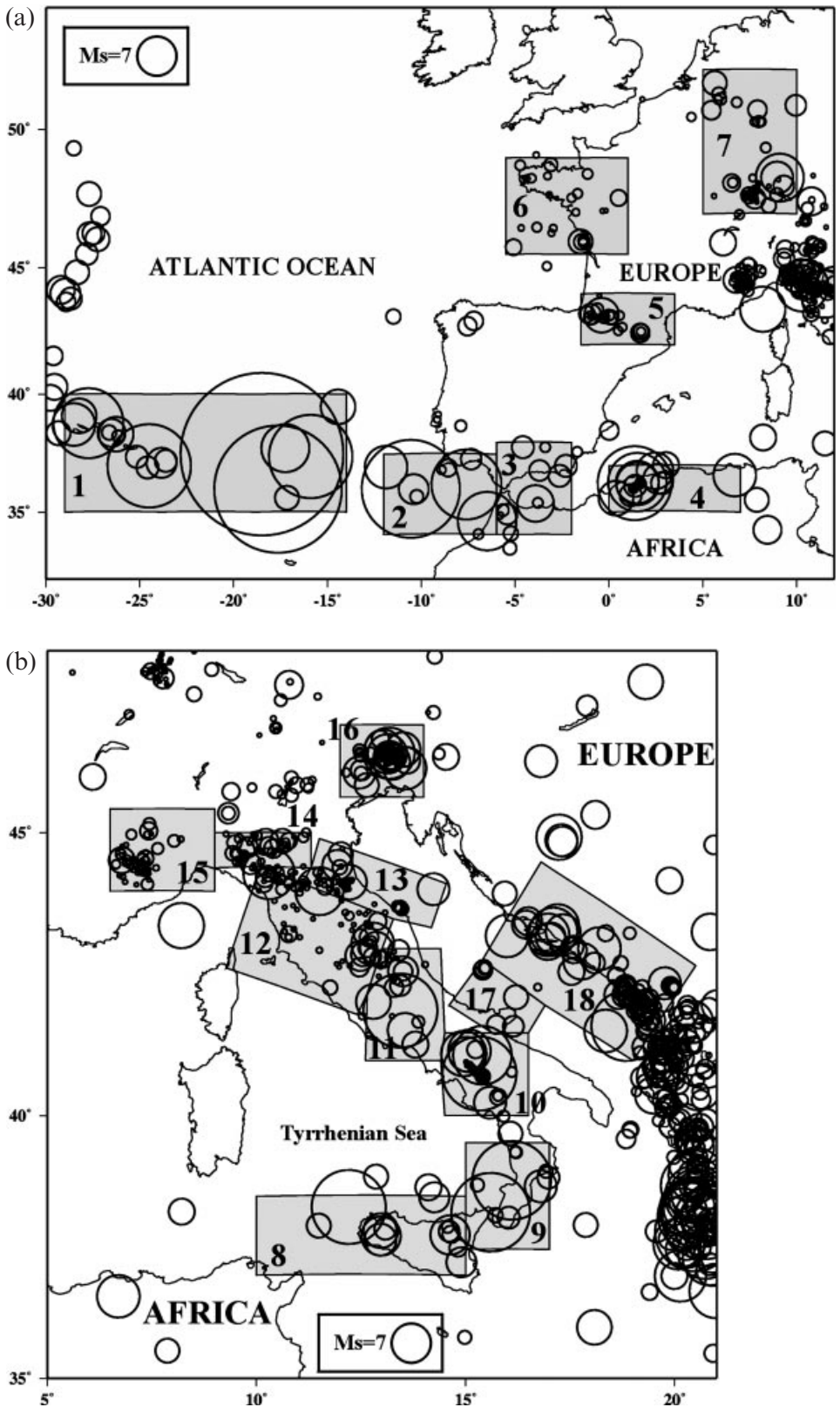

Figure 2. Data distribution and subdivision of the study area into seismic deformation zones. Circles indicate the epicentres of the 2029 earthquakes considered in this study (1905–1999). Circle size is proportional to earthquake magnitude. Geographical name and number of fault plane solutions available for each zone are reported in Table 1. (a) Western Mediterranean, (b) Central Mediterranean, (c) Aegean and (d) Middle East region.

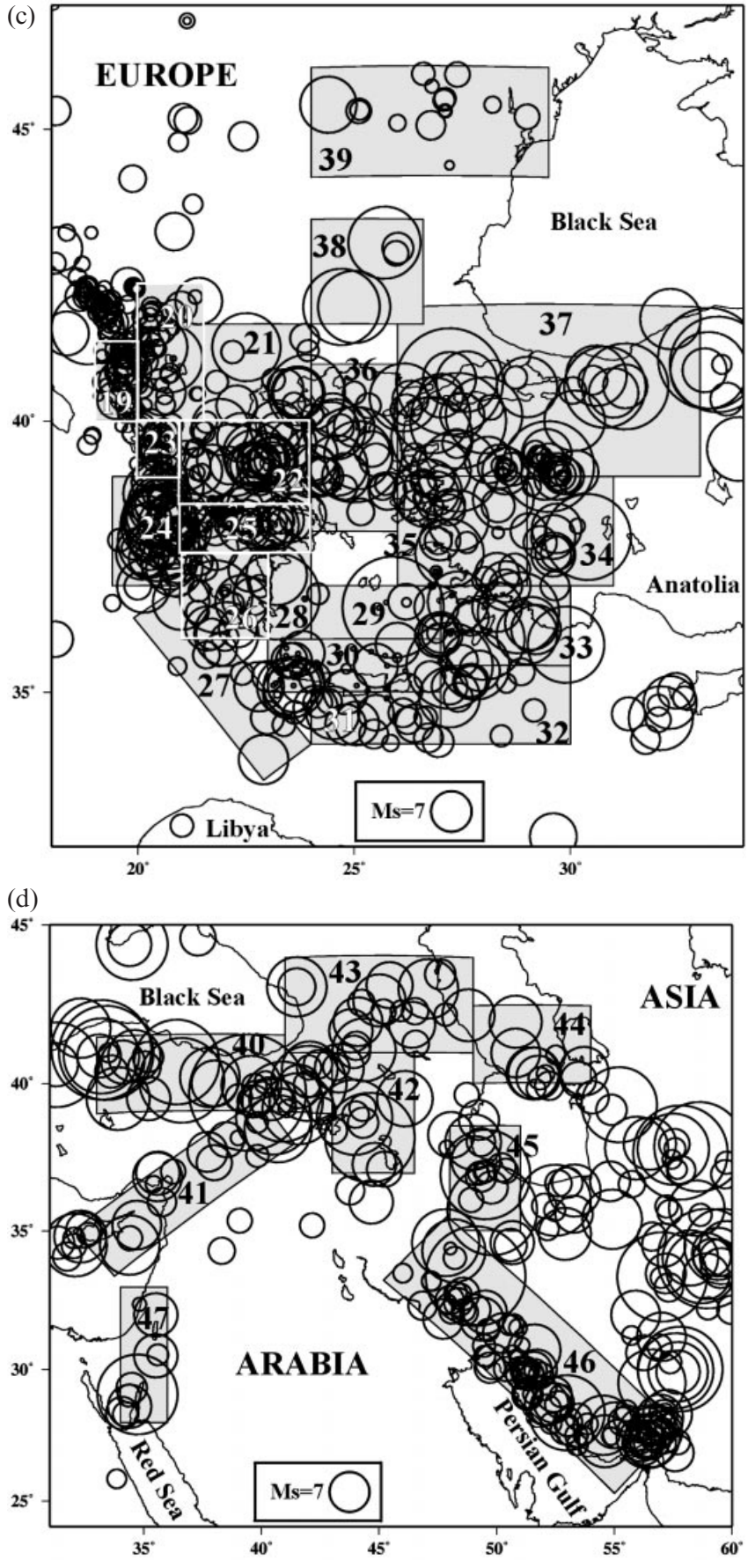

Figure 2. (*Continued.*)

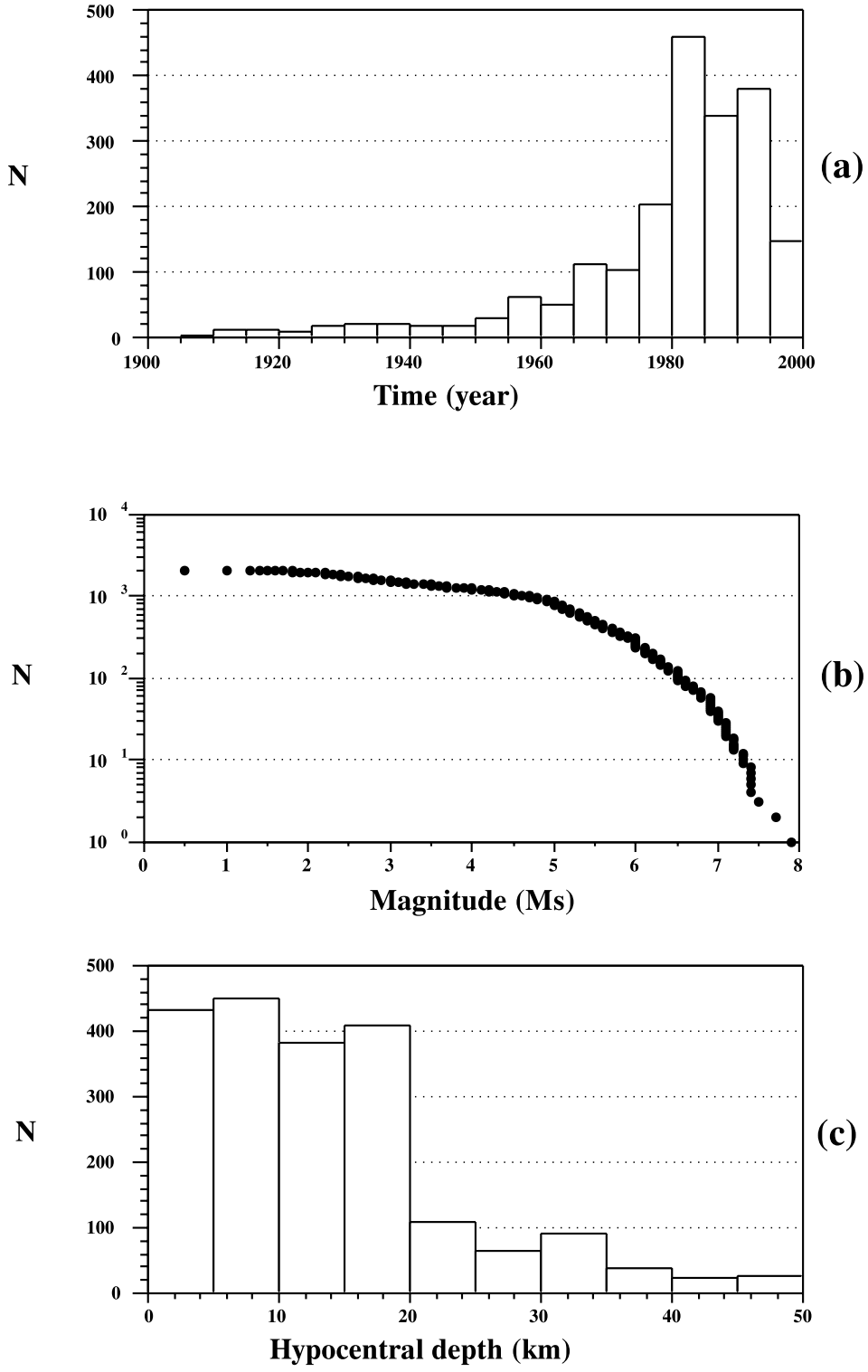

Figure 3. Statistical features of the database. (a) Number of fault plane solutions (N) in 5 yr intervals. The interval 1995–2000 is incomplete, since data stop in March 1999. (b) Cumulative number of fault plane solutions versus surface wave magnitude. N indicates (on a logarithmic scale) the number of events whose magnitude exceeds the value given on the abscissa. The graph may be fitted by a straight line, that is, the data have a distribution compatible with the Gutenberg–Richter relationship, for $M_S > 6.5$ only. This seems to imply incompleteness of the data set for magnitudes lower than the above M_S value (Båth 1983). **(c)** Number of events versus hypocentral depth.

data sets (usually called bootstrap samples or paradata sets), obtained by randomly resampling (with replacements) the original data set, preserve the statistical features of the parent population. Paradata sets can then be used to evaluate (via a distribution-free approach) the statistical properties of a given population parameter by computing the value of that parameter for each paradata set and by analysing the frequency distribution of the values obtained.

In order to apply bootstrap analysis in assessing the uncertainty that affects Kostrov's strain estimates, the N moment tensors available for a given crustal volume are arranged in an array, and N random numbers from 1 to N are generated by a pseudo-random number generator (e.g. Press *et al.* 1986). These numbers are then used to select the corresponding elements of the data array to generate a bootstrap sample. Finally, eq. (3) is applied to this paradata set to compute the strain tensor, along with its principal values and directions. The above procedure is repeated M times. The number M is chosen to provide a reasonable compromise between a satisfactory stability of results and computational effort. As a rough indication, Efron & Tbishirani (1986) suggested a value of $M > 1000$.

The dispersion of the bootstrap values thus obtained may give information on the effect of incomplete sampling of source mechanisms due to the catalogue shortness. This effect can be represented as a confidence limit around relevant parameters (scalar strain ε_0 and directions of the principal axes of strain), taking into account the uppermost and lowermost percentiles (5 and 95 per cent respectively) of the bootstrap sample. These values may be considered as an approximate estimate of the true 95 per cent confidence region.

In order to compute the 95 per cent confidence interval of ε_0 (eq. 4), the values obtained by the bootstrap replications are sorted in increasing order: the 50th and 1950th values are considered representative of the 95 per cent confidence interval. The standard deviation relative to the probability distribution associated with ε_0 can also be obtained from the set of bootstrap replications.

The strain regimes thus obtained in each zone may be illustrated using a representation proposed by Frohlich & Apperson (1992). The orthogonality of the three principal axes of the strain tensor implies that

$$\sin^2(\delta_1) + \sin^2(\delta_2) + \sin^2(\delta_3) = 1\,, \tag{5}$$

where δ_1, δ_2 and δ_3 are the plunges of the maximum, intermediate and minimum lengthening, respectively. Thus, the three principal strains can be represented as a point on a triangle diagram; the distances of each point from the vertices of the triangle indicate the deviation of the corresponding strain pattern from the canonical styles defined above. To evaluate the density of bootstrap solutions within a triangle, the surface of the diagram is divided into 900 equal-area cells, which are ordered on the basis of the number of points belonging to each cell. The lowest tail of this distribution, that is, the cells that cumulatively contain less than the 5 per cent of the bootstrap replications performed, is not represented in the final triangular diagram. The remaining cells, including 95 per cent of the bootstrap population, form the relevant confidence region.

The dispersion on the focal sphere of the principal strain directions obtained by the bootstrap procedure is evaluated by computing the mean resultant length, R (Davis 1986). This parameter is the modulus of the sum of the unit eigenvectors divided by the number of bootstrap replications. Thus R ranges from 0 (unit eigenvectors annihilate one another) to 1 (unit eigenvectors are all parallel).

Stereonets (based on the equal-area zenithal projection) are used to represent the 95 per cent confidence regions for the directions of maximum and minimum lengthening. These diagrams represent the clustering of principal strain directions on the focal sphere. A disconnected confidence region implies that the direction distribution of a given axis is multimodal, that is, more than one family of principal directions is compatible with the available data. Disconnected confidence regions of principal axes could reveal a heterogeneous strain field in the zone involved (Marrett & Allmendinger 1990). As an extreme case, when confidence regions overlap, one could assume that incompatible strain regimes affect that zone. Recognition of more homogeneous subzones might be attempted only if the data set considered is sufficiently large.

DATA ANALYSIS

The first step of the analysis is the identification of crustal volumes to be considered for seismic strain estimates. In order to meet the implicit assumptions underlying Kostrov's approach (eq. 3), the sizes of such volumes should exceed the largest seismic faults they contain. On the other hand, the sizes of these volumes should be sufficiently small to sample nearly homogeneous strain domains in order to allow an univocal tectonic interpretation of strain estimates. By taking these bounds into account, the Mediterranean area has been subdivided into a number of zones, trying to identify as many homogeneous sets of source mechanisms as possible. The choice of the initial geometry of zones has also been based on the analysis of other strain indicators such as morphological and neotectonic information. A lower bound for the size of each crustal domain has been deduced by considering the largest seismic source tentatively estimated from the seismic moment of relevant earthquakes (Wang & Ou 1998). We have then modified, by a trial-and-error procedure, the boundaries of a number of zones, with the final purpose of minimizing the uncertainty that affects the strain style obtained by Kostrov's approach. In particular, we have reconsidered the shapes of the zones when the results obtained suggested an inhomogeneous data set. The level of detail obtainable by progressively reducing the sizes of the zones has been conditioned, in some cases, by the need to have sufficiently large data sets in each crustal volume.

The configuration of zones that we finally adopted is reported in Fig. 2 along with data epicentres. Roughly 30 per cent of zones include less than 15 focal mechanisms, whereas the most populated zones include more than 100 events (Table 1).

For each zone, the permanent strain accommodated by seismic slip in the period 1905–1999 has been computed using eq. (3) by assuming constant values for both thickness (20 km) and average rigidity of the crust ($\mu = 3 \times 10^{10}$ Pa). Different values of the above parameters would merely imply a rescaling of the strain tensor components. The values of ε_0 (eq. 4) in the various zones range from 10^{-11} to 10^{-5} (Table 1). As expected, the lowest values ($< 10^{-8}$) are associated with stable continental domains such as Western Europe and the Adriatic platform (zones 6, 7 and 17 in Figs 2a and b). Small values also characterize the Alboran Sea (3) and some orogenic belts such as the Pyrenees (5), the northeastern Apennines (13) and the western Alps (15). The highest values ($> 10^{-6}$) have been obtained for the central Atlantic (1), the Ionian Islands (24), the Straits of Cythera (28), the Central Aegean Sea (29) and the Northeast Anatolian Fault (40).

In order to determine confidence limits of the results reported in Table 1, bootstrap analysis has been applied to the 47 zones shown in Fig. 2. The number of bootstrap iterations (M) has been fixed at 2000 for each zone, irrespective of the number of available data. The choice of this value is justified by the fact

Table 1. List of the zones considered and average strain tensors obtained by Kostrov's approach applied to the available data. Geographical location of zones is shown in Fig. 2. Numbers in brackets indicate the number of focal mechanisms available in each zone. ε_1, ϕ_1 and δ_1 indicate the eigenvalue (scale factor 10^{-11}), trend (in degrees, positive clockwise from north) and plunge (in degrees, positive towards vertical downwards direction), respectively, of the maximum lengthening axis. ε_2, ϕ_2, δ_2 and ε_3, ϕ_3, δ_3 indicate the eigenvalue, trend and plunge, respectively, of the intermediate lengthening and maximum shortening axes. The last column (Q) shows the uncertainty class assigned to each zone from the bootstrap analysis. Uncertainty level increases from A to D (see text for details).

Zone	ε_1	ϕ_1	δ_1	ε_2	ϕ_2	δ_2	ε_3	ϕ_3	δ_3	Q
(1) Central Atlantic (18)	799744	42	4	−1003	292	78	−798741	133	11	B
(2) Gibraltar (11)	124104	58	75	2274	235	15	−126378	325	1	C
(3) Alboran Sea (12)	549	72	23	−13	185	43	−536	322	38	D
(4) Algeria (91)	38666	304	75	−296	57	6	−38370	149	14	A
(5) Pyrenees (32)	568	43	25	−63	175	55	−505	302	23	D
(6) Brittany (22)	63	71	1	−3	339	62	−60	161	28	A
(7) Rhine Valley (65)	1397	276	37	120	19	17	−1517	130	48	C
(8) Sicily (13)	45957	103	88	1839	271	2	−47796	1	0	C
(9) Calabria (10)	222572	92	2	−58957	359	55	−163615	183	34	C
(10) Southern Italy (171)	151171	45	14	1517	136	3	−152688	238	75	C
(11) Central Italy (27)	99016	22	2	−523	291	35	−98493	114	55	B
(12) Tuscany–Umbria (63)	16585	51	2	−32	321	1	−16553	208	87	A
(13) Northeastern Apennines (70)	3368	151	5	−618	354	85	−2750	241	2	D
(14) North Apennines (41)	1763	203	59	930	73	21	−2693	334	22	C
(15) Western Alps (59)	306	305	3	136	210	57	−442	36	33	D
(16) Friuli (52)	41407	307	58	4377	65	16	−45784	163	26	A
(17) Central Adriatic (8)	760	261	60	−139	76	30	−621	167	2	D
(18) Dalmatia–Montenegro (78)	43583	25	60	643	131	9	−44226	225	28	A
(19) Coastal Albania (38)	24967	50	57	−6979	316	3	−17988	224	33	D
(20) Internal Albania (41)	83397	289	13	−539	21	8	−82858	141	75	D
(21) Macedonia (12)	136942	11	0	7786	101	1	−144728	276	89	A
(22) Thessaly (45)	152991	26	5	27872	296	5	−180863	164	83	A
(23) Epirus (30)	10129	306	81	151	139	9	−10280	48	2	C
(24) Ionian Islands (49)	619541	14	79	−12558	150	8	−606983	241	8	A
(25) Gulf of Corinth (197)	94883	185	9	−385	93	12	−94498	310	75	A
(26) Peloponnesus (14)	96305	38	74	4970	130	1	−101275	220	16	C
(27) West Hellenic Trench (12)	22652	51	75	−8937	300	5	−13715	208	14	B
(28) Straits of Cythera (4)	437625	246	0	20123	156	0	−457748	8	90	B
(29) Central Aegean Sea (14)	606794	330	5	5856	60	0	−612650	154	85	C
(30) Crete (43)	65500	30	63	1060	121	0	−66560	211	27	A
(31) Central Hellenic Trench (16)	23826	355	62	−4879	250	8	−18947	156	26	A
(32) East Hellenic Trench (11)	21319	23	73	−1243	114	0	−20076	204	17	C
(33) Rhodes (20)	239046	313	67	206012	104	20	−445058	198	10	C
(34) Burdur (11)	175255	145	4	6531	235	9	−181786	32	81	B
(35) West Turkey (30)	93334	184	1	−23655	274	1	−69679	46	88	A
(36) North Aegean Trough (23)	285070	167	14	−12485	302	70	−272585	73	13	A
(37) Northwest Anatolian Fault (68)	289182	8	0	−54507	99	23	−234675	278	67	C
(38) Bulgaria (5)	254767	200	0	13374	290	0	−268141	81	90	A
(39) Romania (15)	6944	180	0	−391	270	2	−6553	76	88	D
(40) Northeast Anatolian Fault (35)	443863	237	1	5172	6	89	−449035	147	1	A
(41) Southeast Anatolian Fault (19)	10401	92	52	6727	289	37	−17128	193	8	C
(42) Turkey–Iran border region (11)	67515	246	0	−12160	336	60	−55355	156	30	A
(43) Caucasus (19)	19407	290	71	−2349	103	19	−17058	194	2	A
(44) North Caspian Sea (10)	10779	1	62	722	124	16	−11501	221	23	A
(45) Northwest Iran (14)	170597	164	58	9811	320	29	−180408	56	11	B
(46) Zagros Chain (98)	21482	21	87	18266	274	1	−39748	184	3	C
(47) Dead Sea Fault (10)	57979	62	12	−489	314	55	−57490	160	32	D

that tests carried out in selected zones indicate that the computed confidence limits do not show significant changes as M varies within the range 1000–10 000.

The 95 per cent confidence intervals obtained for ε_0 are shown in Fig. 4. These intervals should be interpreted as an assessment of the long-term variability of the incremental strain in the various zones induced by catalogue shortness. The degree of clustering of the bootstrap principal axes is shown in Fig. 5 in terms of the parameter R. Figs 6, 7, 8 and 9 show the 95 per cent confidence regions for the strain regimes of the zones considered in the form of both triangular diagrams and stereonets.

MAIN RESULTS

The results shown in Figs 4–9 have been tentatively divided into four classes (A, B, C and D) to organize their description better. The quality of the results, that is, the level at which

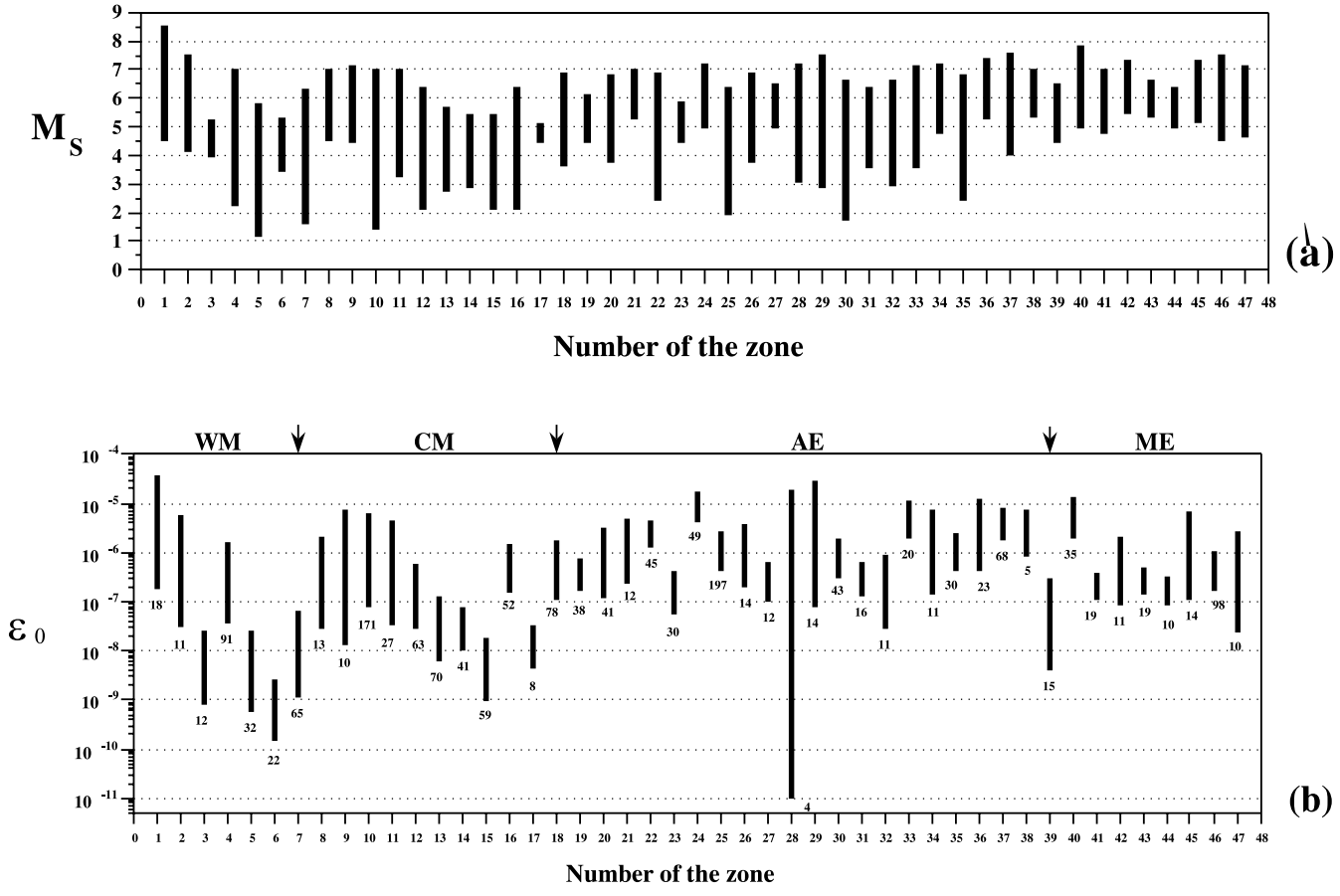

Figure 4. Uncertainty in scalar strain. (a) Magnitude range (M_S) of the earthquakes considered in each deformation zone. (b) 95 per cent confidence interval of the scalar strain (ε_0) defined by eq. (4). Numbers on the horizontal axis correspond to zones shown in Fig. 2. Abbreviations indicate the regions shown in Figs 2 and 6–9 (WM: western Mediterranean; CM: central Mediterranean; AE: Aegean region; ME: Middle East). The number of data available in each zone are reported below the interval bar.

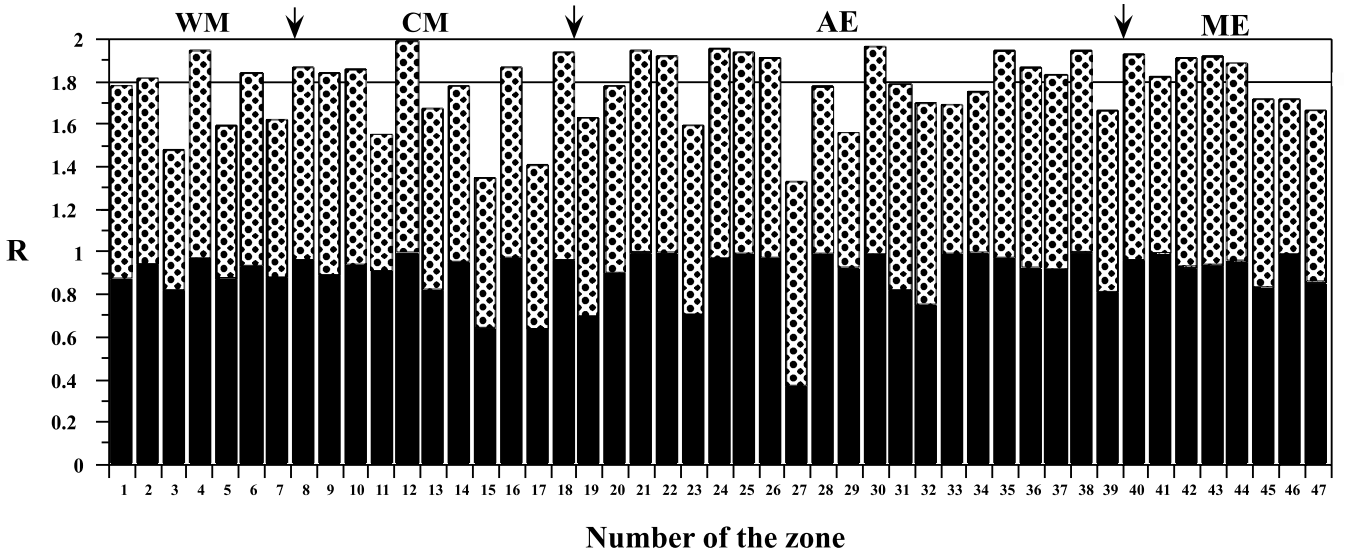

Figure 5. Dispersion of the directions of principal axes for the 2000 bootstrap strain tensors computed for each zone. Abbreviations of regions are the same as in Fig. 4. Dotted and black columns indicate the value of the dispersion index R (see text) for the maximum and minimum lengthening axes, respectively. The horizontal line corresponding to the value $R = 1.8$ indicates the decision level adopted to assign a given strain estimate to quality class A (see text).

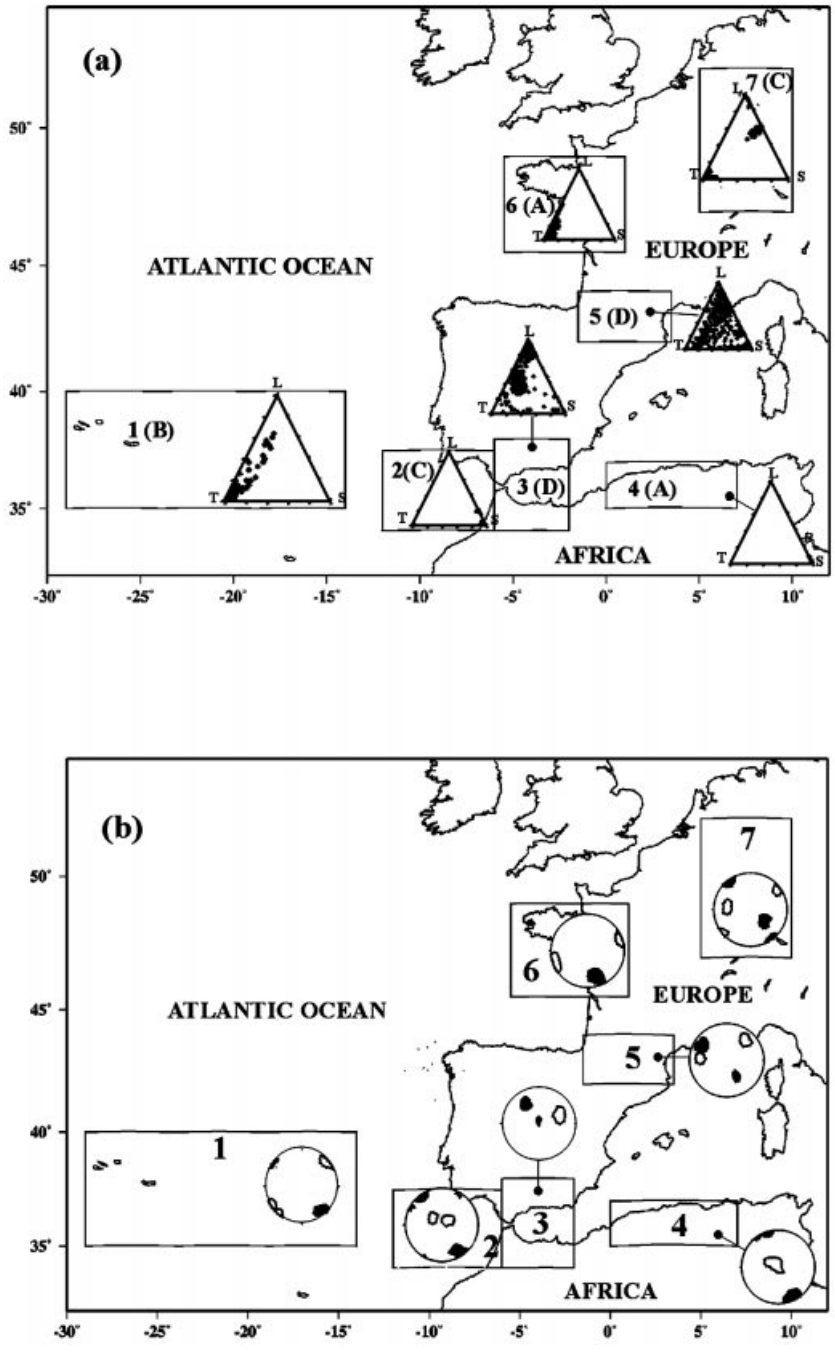

Figure 6. Uncertainty on strain style for the western Mediterranean region. (a) Triangle diagrams for zones 1–7. The vertices of each triangle correspond to the three canonical strain styles defined in the text (L = lengthening, T = transform, S = shortening). Black points within the diagrams represent the 95 per cent confidence region of the 2000 bootstrap strain tensors computed for each zone (see text for explanation). The quality class of each zone is given in brackets beside the zone number. (b) Stereonets for zones 1–7. Equal-area zenithal projections of the 95 per cent confidence regions of two principal axes computed for each zone from the bootstrap population of 2000 strain tensors. White and black areas refer to the maximum and minimum lengthening axes (ε_1 and ε_3, respectively).

strain regimes are constrained, decreases from class A to class D. The uncertainty on scalar strains (Fig. 4) is discussed separately. Obviously, we are aware that the proposed classification is not unique and that it cannot account for the entire information contained in the results of the bootstrap analysis.

Class A includes the zones for which the confidence region in the triangle diagram includes one vertex only, implying that one strain style is associated with these zones and the other two styles may be ruled out. Furthermore, the sum of the *R*-values for the maximum and minimum lengthening axes must be greater than 1.8 (Fig. 5). This last requisite implies that the dispersion on the focal sphere of the above principal axes is low, that is, the directions of principal strains are fairly well constrained. Class B includes the zones for which a strain style can be recognized by the triangle diagrams, but the sum of the *R*-values for the above principal axes is lower than 1.8 (Fig. 5). Class C refers to the zones for which the confidence region in the triangle diagram includes two vertices. In this case, the only

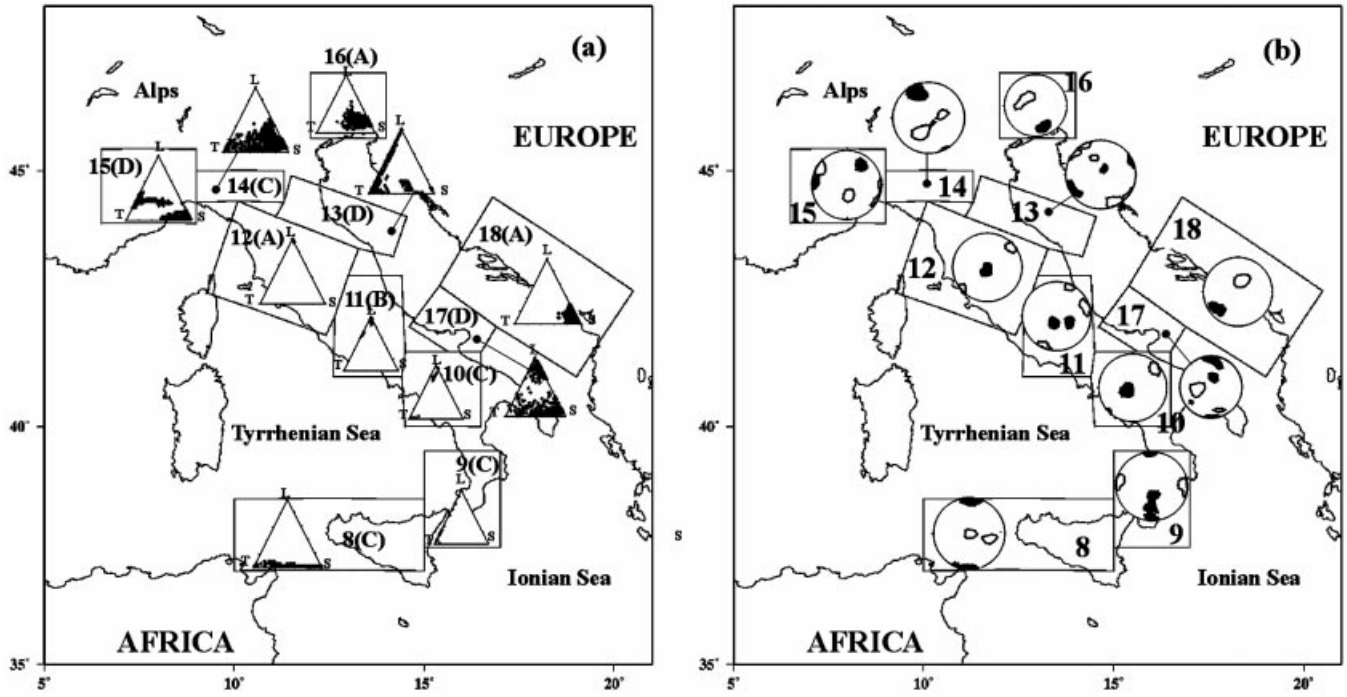

Figure 7. Uncertainty on strain style for the central Mediterranean region. (a) Triangle diagrams and (b) stereonets for zones 8–18 (see caption to Fig. 6).

constraint is that one strain style can be ruled out for the zone considered. Finally, class D includes the zones for which no clear indication of strain regime can be derived. Table 1 reports the uncertainty class assigned to each zone of Fig. 2.

For six zones (10, 23, 26, 29, 32 and 37), the strain style indicated by the triangle diagram does not correspond to any family of principal axes in the corresponding stereonet (see Figs 6–9). This difference depends on the fact that 5 per cent of

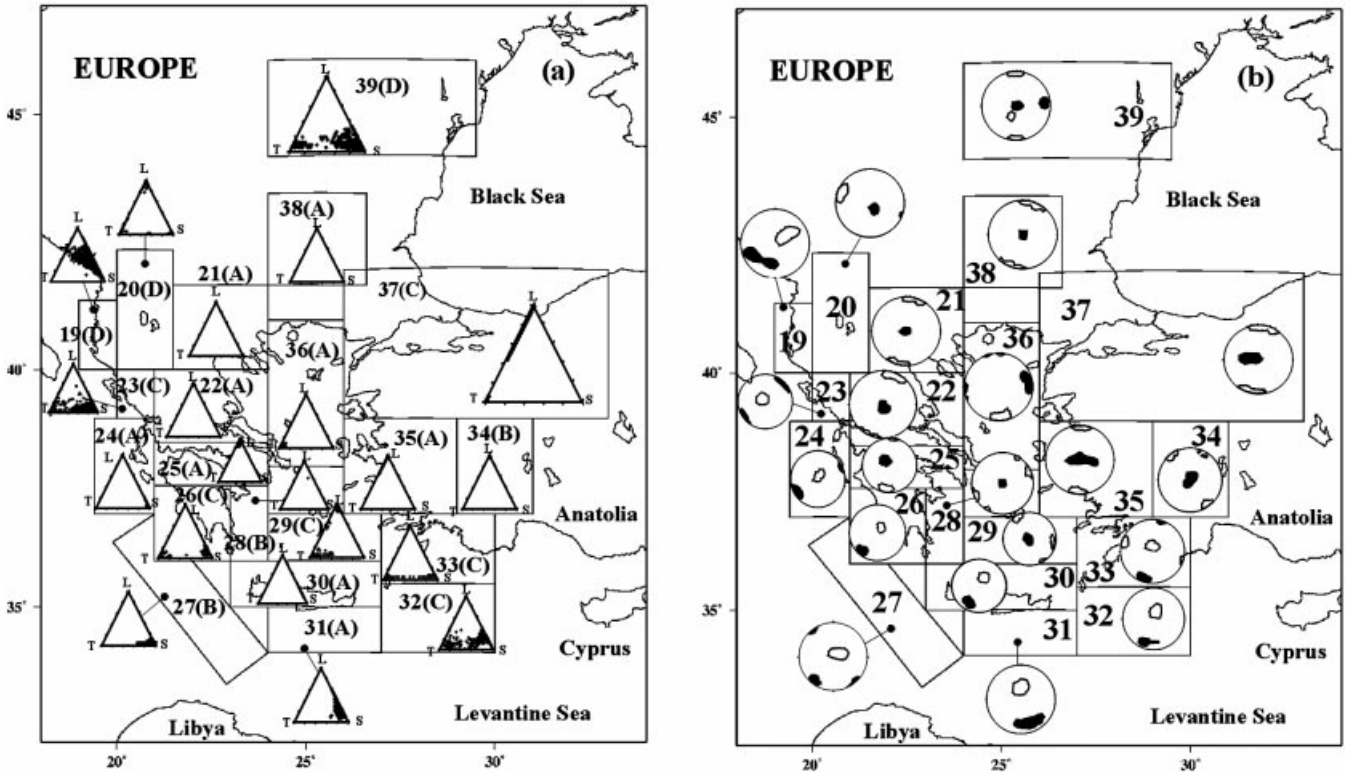

Figure 8. Uncertainty on strain style for the Aegean region. (a) Triangle diagrams and (b) stereonets for zones 19–39 (see caption to Fig. 6).

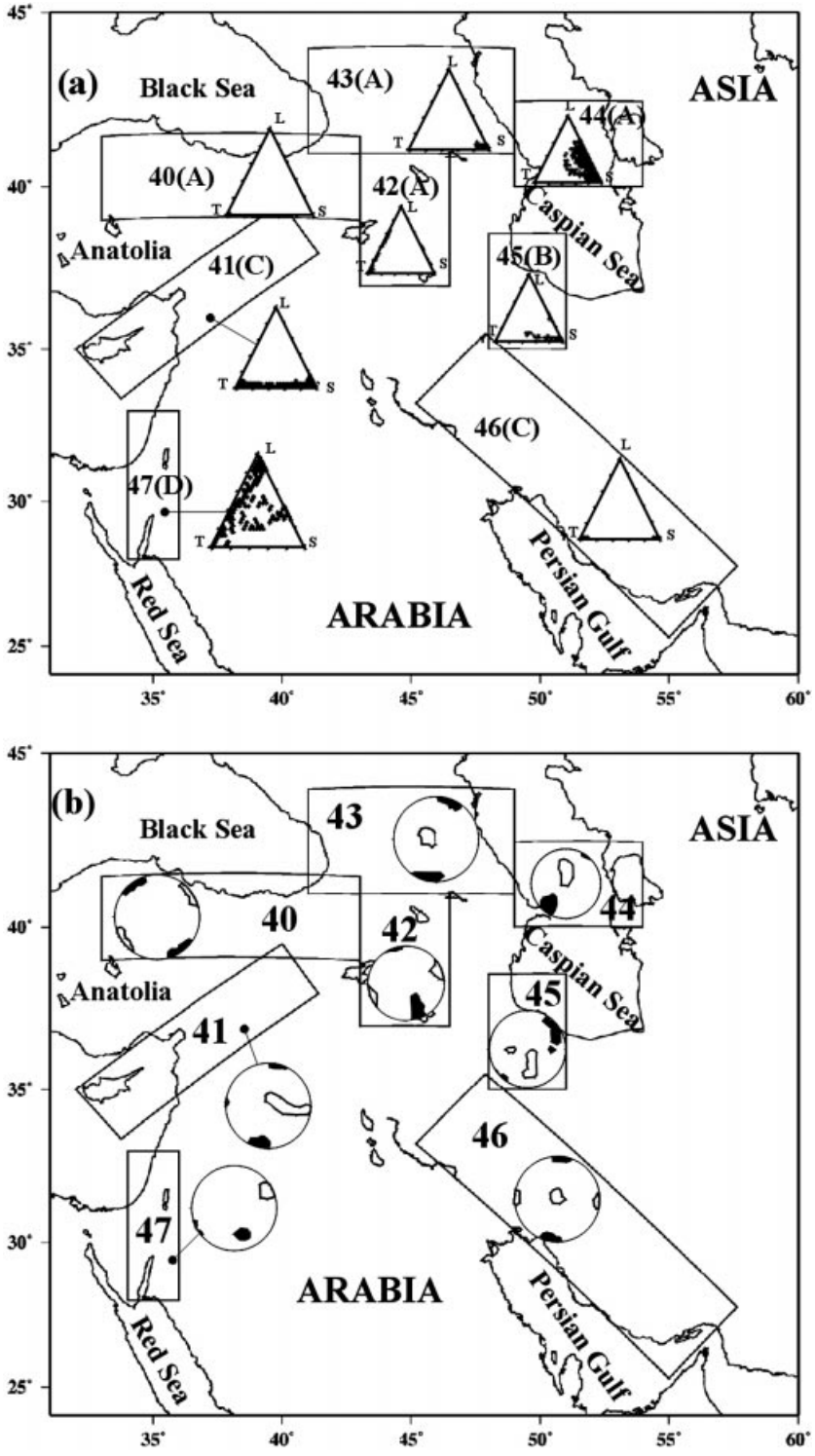

Figure 9. Uncertainty on strain style for the Middle East region. (a) Triangle diagrams and (b) stereonets for zones 40–47 (see caption to Fig. 6).

the principal strain axes do not belong to the related confidence regions, being scattered on the focal sphere. However, even scattered axes might correspond to a univocally defined strain style in the triangle diagram. Thus, a confidence region in the triangle diagram may include strain tensors not reported in the related stereonet, since they contribute to define a possible strain style in the zone involved but do not give information on the directions of principal strains.

Western Mediterranean

Seismic activity concentrates in a relatively narrow belt between the Azores and Algeria, south of 40°N, as indicated by the fact that scalar strains in the central Atlantic, western Atlantic and Algeria (zones 1, 2 and 4) are two orders of magnitude greater than in the remaining western Mediterranean zones (Fig. 4).

Values of R, triangle diagrams and stereonets (Figs 5, 6a and 6b, respectively) suggest that two zones can be included in class A: Algeria (4), characterized by NW–SE shortening, and Brittany (6), which shows a transform style, with NW–SE shortening and NE–SW lengthening. Class B includes only the central Atlantic (1), with a right-lateral transform style. Class C includes the Gibraltar zone (2) and the Rhine Valley (7), where lengthening and shortening styles can be excluded, respectively. The strain field is very poorly constrained (class D) in the remaining two zones, i.e. the Alboran Sea (3) and the Pyrenees (5).

Central Mediterranean

In the Italian peninsula (zones 8–15) scalar strains show a significant and systematic decrease from south to north (Fig. 4). The largest values ($>10^{-8}$) are at the northeastern boundary of the Adriatic plate (zones 16 and 18). In general it is noted that a large uncertainty, scattered over two or three orders of magnitude, affects scalar strains. Information on strain regimes is indicated in Figs 5, 7(a) and 7(b).

Class A includes only three zones: Tuscany–Umbria (12), with NE–SW lengthening, Friuli (16), with roughly N–S shortening, and Dalmatia–Montenegro (18), with NE–SW shortening. Class B includes central Italy (11), where a lengthening style can be recognized in Fig. 7(a). Class C includes four zones: Sicily (8), with an undefined combination of shortening and transform styles, the northern Apennines (14), for which lengthening can be ruled out, Calabria (9) and Southern Italy (10), where shortening is not compatible with data. The remaining zones, i.e. the northeastern Apennines (13), western Alps (15) and central Adriatic (17), are classified as D.

Aegean region

In most zones scalar strains are larger than 10^{-8} and, in some cases (zones 24, 33, 36, 37 and 38), they reach values larger than 10^{-6} (Fig. 4). The lowest value is in Romania (39), located within the Eurasian foreland, while the highest value is in the central Aegean Sea (29). The Straits of Cythera (28) show the largest uncertainty among the tectonic belts we have considered in this work.

Nine zones can be classified as class A (Figs 5, 8a and 8b): the Ionian Islands (24), with NE–SW shortening, Crete (30) and the central Hellenic Trench (31), with NNE–SSW to NNW–SSE shortening, Macedonia (21), Thessaly (22), the Gulf of Corinth (25), Bulgaria (38) and western Turkey (35), with a N–S lengthening, and the north Aegean Trough (36), characterized by a right-lateral transform style. Class B includes three zones: the western Hellenic trench (27), affected by shortening, the Straits of Cythera (28) and the Burdur zone (34), both affected by lengthening. Class C includes six zones: Epirus (23), the Peloponnesus (26), the eastern Hellenic Trench (32), where lengthening can be ruled out, Rhodes (33), where a combination of shortening and transform styles occurs, the central Aegean Sea (29) and the western sector of the North Anatolian Fault (37), where shortening can be excluded. Finally, the strain regime is poorly defined (class D) in both coastal (19) and internal Albania (20) and in Romania (39).

Middle East

The largest scalar strains ($>10^{-6}$) occur in the eastern sector of the North Anatolian Fault (40) and in northwestern Iran (45), as indicated in Fig. 4.

Concerning strain regimes (Figs 5, 9a and 9b), Class A includes four zones: the eastern sector of the North Anatolian Fault (40), characterized by a right-lateral transform style; the Turkey–Iran border region (42), where a transform regime prevails with N–S shortening, and the Caucasus (43) and the central Caspian Sea (44), where N–S to NE–SW shortening occurs. Class B includes northwestern Iran (45), affected by shortening. Class C includes the southeast Anatolian Fault (41), with a combination of shortening and transform styles, and the Zagros orogenic belt (46), in which the lengthening style can be excluded. The Dead Sea zone (47) is assigned to the last class (D).

DISCUSSION AND CONCLUSIONS

The reliability of seismic strain estimates carried out by Kostrov's approach cannot easily be evaluated, since the related level of uncertainty, due to the random occurrence of earthquakes in time, experimental errors, catalogue shortness and incompleteness, and the non-fulfilment of some basic conditions (such as the homogeneity of the strain regime and the actual significance of the available data set in the zone considered), is generally poorly known. An attempt to gain insight into the above problem has been made by applying an empirical resampling technique (bootstrap) to 47 active zones over the entire Mediterranean area.

Previous results suggest that experimental errors and catalogue incompleteness for minor earthquakes make a minor contribution to uncertainty in long-term strain estimates with respect to earthquake randomness. The results obtained here suggest that the effect of the possibly incomplete sampling of major earthquakes in the average strain estimates (due to catalogue shortness) dominates over other sources of uncertainty. To stress this point, standard deviations of the Euclidean norm (eq. 4) of the average bootstrap strain tensors have been compared with those obtained by taking into account only the effect of the random time distribution of earthquakes (Fig. 10). This comparison clearly shows that the effect of the catalogue shortness in almost all cases exceeds, by several orders of magnitude, the effect of randomness in the time occurrence of earthquakes.

The spreading of strain tensors obtained from paradata sets (deduced by resampling original data samples) has been used to determine tentative confidence limits of deformation styles and principal strain directions for each zone. The results obtained have been ranked in four classes (A to D), with an increasing level of ambiguity. The highest quality (class A) has been assigned to the 18 zones where both the strain style and the horizontal directions of principal strains can be recognized. A lower quality (class B) has been attributed to six zones, where only the strain style can be inferred from triangle diagrams. Much higher ambiguity characterizes the 23 zones included in the last two classes (C and D). This result indicates that, in spite of our efforts to subdivide the study area based on the most homogeneous distribution of focal mechanisms, the deformation style cannot be clearly recognized in roughly half of the

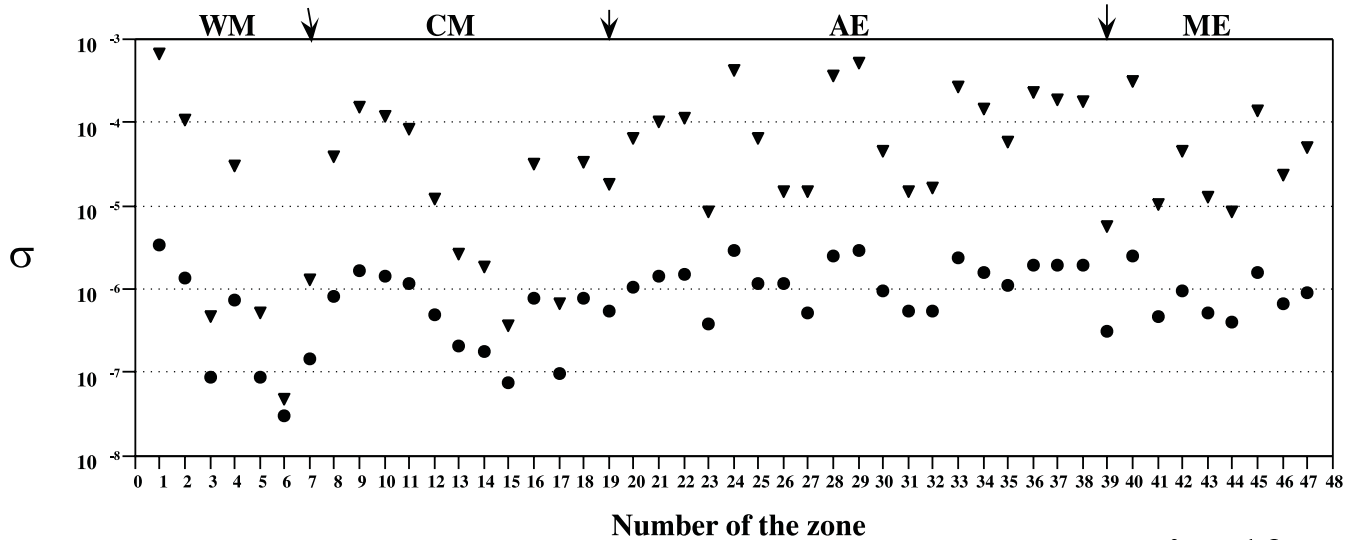

Figure 10. Comparison of uncertainty induced in scalar strain (eq. 4) by catalogue shortness (triangles) and randomness in time occurrence of earthquakes (circles). For each seismic zone, a standard deviation (σ), representative of the effect of the catalogue shortness, has been computed using paradata sets from bootstrap iterations (triangles). The standard deviation associated with the randomness in occurrence time of earthquakes has been obtained from original data through the procedure proposed by Shen-Tu *et al.* (1998).

zones investigated, mostly located in the western and central Mediterranean regions. Moreover, large uncertainties, even reaching some orders of magnitude, have been estimated for scalar strains. This suggests that one should be cautious in using the results of Kostrov's analysis as constraints on tectonic processes in the study area.

In order to understand to what extent the ambiguity of strain depends on the reliability of data sets, some statistical tests have been carried out. In particular, we have explored how the composition of data sets in the various zones, such as the number and age of events, may have influenced the quality of the results. Since the size of the original data set may affect the accuracy of the bootstrap confidence limits (Fisher 1993), one could expect that data sets in 'high-quality' zones are systematically larger than those in 'low-quality' zones. This idea, however, is not confirmed by the results of a non-parametric test (Kendall 1970), which suggest that no significant correlation exists between uncertainty level and number of events in the data set. One may also suspect that the exclusion of older events, whose fault plane solutions are presumably less well constrained than those of recent earthquakes, would allow a better constraint of deformation styles. However, Kendall's test shows a significant (<0.05) negative correlation between the uncertainty level and the percentage of pre-1960 events in the zones considered, and thus suggests that the reliability of the seismic strain estimate increases with the length of the time interval covered by the data set. These results seem to favour the hypothesis that the ambiguity in seismic strain estimates for many segments of the Mediterranean region is not related to data quality, but rather reflects the lack of capability of the available data set to resolve the high strain field heterogeneity in the zones involved.

ACKNOWLEDGMENTS

We are very grateful to M. L. Jost and to an anonymous reviewer for very useful suggestions about basic aspects of our approach and the organization of the work. We are also grateful to Dr F. D'Onza for valuable help given in drawing the figures. Figs 2 and 6–9 were drawn with the GMT shareware software (Wessel & Smith 1995). This research has been supported by the Italian Ministry of University and Scientific Research (MURST).

REFERENCES

Albarello, D., 2000. A resampling approach to test stress-field uniformity from fault data, *Geophys. J. Int.,* **140,** 535–542.

Amelung, F. & King, G., 1997. Large-scale tectonic deformation inferred from small earthquakes, *Nature,* **386,** 702–705.

Amoruso, A., Crescentini, L. & Scarpa, R., 1998. Inversion of source parameters from near- and far-field observations: an application to the 1915 Fucino earthquake, central Apennines, Italy, *J. geophys. Res.,* **103,** 29 989–29 999.

Anderson, H. & Jackson, J., 1987. Active tectonics of the Adriatic region, *Geophys. J. R. astr. Soc.,* **91,** 937–983.

Baker, C., Jackson, J. & Priestley, K., 1993. Earthquakes on the Kazerun Line in the Zagros Mountain of Iran: strike-slip faulting within a fold-and-thrust belt, *Geophys. J. Int.,* **115,** 41–61.

Baker, C., Hatzfeldt, D., Lyon-Caen, H., Papadimitriou, E. & Rigo, A., 1997. Earthquake mechanisms of the Adriatic Sea and western Greece: implications for the oceanic subduction–continental collision transition, *Geophys. J. Int.,* **131,** 559–594.

Båth, M., 1983. Earthquake data analysis: an example from Sweden, *Earth Sci. Rev.,* **19,** 181–303.

Bernard, P., Gariel, J.-C. & Dorbath, L., 1997. Fault location and rupture kinematics of the magnitude 6.8, 1992 Erzincan earthquake, Turkey, from strong ground motion and regional records, *Bull. seism. Soc. Am.,* **87,** 1230–1243.

Bonjer, K.-P., 1997. Seismicity pattern and style of seismic faulting at the eastern borderfault of the southern Rhine Graben, *Tectonophysics,* **275,** 41–69.

Boore, D., Sims, J., Kanamori, H. & Harding, S., 1981. The Montenegro, Yugoslavia, earthquake of April 15, 1979: source orientation and strength, *Phys. Earth planet. Inter.,* **27,** 133–142.

Buforn, E., Udias, A. & Mezcua, J., 1988. Seismicity and focal mechanisms in South Spain, *Bull. seism. Soc. Am.,* **78,** 2008–2024.

Cipar, J., 1981. Broadband time domain modelling of earthquakes from Friuli, Italy, *Tectonophysics,* **71,** 1215–1231.

Davis, J.C., 1986. *Statistics and Data Analysis in Geology,* John Wiley, New York.

Dercourt, J. *et al.*, 1986. Geological evolution of the Tethys belt from Atlantic to the Pamirs since the Lias, *Tectonophysics,* **123,** 241–315.

Deschamps, A. & King, G.C.P., 1984. Aftershocks of the Campania-Lucania (Italy) earthquake of 23 November, 1980, *Bull. seism. Soc. Am.,* **74,** 2483–2517.

Dziewonski, A.M. & Woodhouse, J.H., 1983. An experiment in systematic study of global seismicity: centroid-moment tensor solutions for 201 moderate and large earthquakes of 1981, *J. geophys. Res.,* **88,** 3247–3271.

Dziewonski, A.M., Friedman, A. & Woodhouse, J.H., 1983. Centroid moment tensor solutions for January–March, 1983, *Phys. Earth planet. Inter.,* **33,** 71–75.

Efron, B. & Tbishirani, R.J., 1986. Bootstrap methods for standard errors, confidence intervals and other measures of statistical accuracy, *Stat. Sci.,* **1,** 54–77.

Ekström, G. & England, P., 1989. Seismic strain rates in regions of distributed continental deformation, *J. geophys. Res.,* **94,** 10 231–10 257.

Ekström, E. & Nettles, M., 1997. Calibration of the HGLP seismograph network and centroid-moment tensor analysis of significant earthquakes of 1976, *Phys. Earth planet. Inter.,* **101,** 219–243.

Eva, E. & Pastore, S., 1993. Revisione dei meccanismi focali dell'Appennino settentrionale, *Proc. 12th GNGTS Mtng*, pp. 147–159, Esagrafica, Roma, Italy.

Eva, C., Riuscetti, M. & Slejko, D., 1988. Seismicity of the Black Sea region, *Boll. Geof. Teor. Appl.,* **30,** 53–66.

Eva, E., Solarino, S., Eva, C. & Neri, G., 1997. Stress tensor orientation derived from fault plane solutions in the south-western Alps, *J. geophys. Res.,* **102,** 8171–8185.

Eyidogan, H., 1988. Rates of crustal deformation in western Turkey as deduced from major earthquakes, *Tectonophysics,* **148,** 83–92.

Eyidogan, H. & Jackson, J., 1985. A seismological study of normal faulting in the Demirci, Alasehir and Gediz earthquakes of 1969–1970 in western Turkey: implications for the nature and geometry of deformation in the continental crust, *Geophys. J. R. astr. Soc.,* **81,** 569–607.

Fisher, N.I., 1993. *Statistical Analysis of Circular Data,* Cambridge University Press, Cambridge.

Frepoli, A. & Amato, A., 1997. Contemporaneous extension and compression in the northern Apennines from earthquake fault-plane solutions, *Geophys. J. Int.,* **129,** 368–388.

Frohlich, C. & Apperson, D., 1992. Earthquake focal mechanisms, moment tensors, and the consistency of the seismic activity near plate boundaries, *Tectonics,* **11,** 279–296.

Gallart, J., Daignières, M., Gagnepain-Beyneix, J. & Hirn, A., 1985. Relationship between deep structure and seismicity in the western Pyrenees, *Ann. Geophys.,* **3,** 239–248.

Gasparini, C., Iannaccone, G. & Scarpa, R., 1985. Fault-plane solutions and seismicity of the Italian peninsula, *Tectonophysics,* **117,** 59–78.

Giardini, D., Dziewonski, A.M. & Woodhouse, J.H., 1985. Centroid-moment tensor solutions for 113 large earthquakes in 1977–1980, *Phys. Earth planet. Inter.,* **40,** 259–272.

Grimison, N.L. & Chen, W.P., 1988. Source mechanisms of four recent earthquakes along the Azores–Gibraltar plate boundary, *Geophys. J.,* **92,** 391–401.

Grunthal, G. & Stromeyer, D., 1992. The recent crustal stress field in central Europe: trajectories and finite element modeling, *J. geophys. Res.,* **97,** 11 805–11 820.

Hall, P., 1992. *The Bootstrap and Edgeworth Expansion,* Springer-Verlag, New York.

Hatzfeld, D., Besnard, M., Makropoulos, K. & Hatzidimitriou, P., 1993. Microearthquake seismicity and fault-plane solutions in the southern Aegean and its geodynamic implications, *Geophys. J. Int.,* **115,** 799–818.

Jackson, J. & McKenzie, D., 1988. The relationship between plate motions and seismic moment tensors, and the rates of active deformation in the Mediterranean and Middle East, *Geophys. J.,* **93,** 45–73.

Jackson, J., Haines, J. & Holt, W., 1992. The horizontal velocity field in the deforming Aegean Sea region determined from the moment tensors of earthquakes, *J. geophys. Res.,* **97,** 17 657–17 684.

Jost, M.L. & Herrmann, R.B., 1989. A student's guide to and review of moment tensors, *Seism. Res. Lett.,* **60,** 37–57.

Kahle, H.-G. *et al.*, 1998. The strain rate field in the eastern Mediterranean region, estimated by repeated GPS measurements, *Tectonophysics,* **294,** 237–252.

Kahle, H.-G. *et al.*, 1999. The GPS strain rate field in the Aegean Sea and Western Anatolia, *Geophys. Res. Lett.,* **26,** 2513–2516.

Kahle, H.-G., Cocard, M., Peter, Y., Geiger, A., Reilinger, R., Barka, A. & Veis, G., 2000. GPS-derived strain rate field within the boundary zones of the Eurasian, African and Arabian plates, *J. geophys. Res.,* **105,** 23 353–23 370.

Karakaisis, G.F., Karacostas, B.G., Scordilis, E.M., Kiratzi, A.A., Diagourtas, D., Papadimitriou, P., Voulgaris, N. & Ziazia, M., 1993. The spatial distribution of the aftershocks and the focal mechanism of the Galaxidi earthquake (central Greece), *Proc 2nd Congr. Hell. Geophys. Un.,* pp. 309–317, Florina, Greece.

Kasahara, K., 1981. *Earthquake Mechanics,* Cambridge University Press, Cambridge.

Kendall, M.G., 1970. *Rank Correlation Methods,* Griffin, London.

Kiratzi, A., 1991. Rates of crustal deformation in the north Aegean trough-north Anatolian fault deduced from seismicity, *Pure appl. Geophys.,* **136,** 421–432.

Kiratzi, A., 1993. A study on the active crustal deformation of the north and east Anatolian fault zones, *Tectonophysics,* **225,** 191–203.

Kiratzi, A., 1999. Stress tensor inversion in Western Greece using earthquake focal mechanisms from the Kozani-Grevena 1995 seismic sequence, *Ann. Geofis.,* **42,** 725–734.

Kiratzi, A. & Langston, C., 1989. Estimation of earthquake source parameters of the May 4, 1972 event of the Hellenic arc by the inversion of waveform data, *Phys. Earth planet. Inter.,* **57,** 225–232.

Kiratzi, A., Wagner, G. & Langston, C., 1991. Source parameters of some large earthquakes in northern Aegean determined by body waveform inversion, *Pure appl. Geophys.,* **135,** 515–527.

Kostrov, V.V., 1974. Seismic moment and energy of earthquakes, and seismic flow of rock, *Izv. Acad. Sci. USSR Phys. Solid Earth,* **1,** 23–44.

Larson, E., 1999. *On-Line CMT Catalog,* Harvard University (http://www.seismology.harvard.edu/CMTsearch.html).

Liotier, Y., 1989. Modelisation des ondes de Volume ses seismes de l'arc Egeen, *Formation de 3e Cycle,* UFR de Mechanique, Universite Joseph Fourier de Grenoble 1, Grenoble.

Lundgren, P., Giardini, D. & Russo, R.M., 1998. A geodynamic framework for eastern Mediterranean kinematics, *Geophys. Res. Lett.,* **25,** 4007–4010.

Lyon-Caen, H. *et al.*, 1988. The 1986 Kalamata (south Peloponnesus) earthquake: detailed study of a normal fault, evidence for east–west extension in the Hellenic arc, *J. geophys. Res.,* **93,** 14 967–15 000.

Mantovani, E., Albarello, D., Tamburelli, C., Babbucci, D. & Viti, M., 1997. Plate convergence, crustal delamination, extrusion tectonics and minimization of shortening work as main controlling factors of the recent Mediterranean deformation pattern, *Ann. Geofis.,* **40,** 611–643.

Mantovani, E., Albarello, D., Babbucci, D., Tamburelli, C. & Viti, M., 2000a. Genetic mechanism of back-arc opening: insights from the Mediterranean deformation pattern, in *Problems in Geophysics for the New Millennium,* pp. 151–178, eds Boschi, E., Ekström, G. & Morelli, A., Istituto Nazionale Di Geofisica, Roma, Italy.

Mantovani, E., Viti, M., Albarello, D., Tamburelli, C., Babbucci, D. & Cenni, N., 2000b. Role of kinematically induced horizontal forces in Mediterranean tectonics: insights from numerical modeling, *J. Geodyn.,* **30,** 287–320.

Mantovani, E., Cenni, N., Albarello, D., Viti, M., Babbucci, D., Tamburelli, C. & D'Onza, F., 2001. Numerical simulation of the observed strain field in the central-eastern Mediterranean region, *J. Geodyn.,* in press.

Marrett, R. & Allmendinger, R.W., 1990. Kinematic analysis of fault-slip data, *J. struct. Geol.,* **12,** 973–986.

Marrett, R. & Allmendinger, R.W., 1992. Amount of extension on small faults: an example from the Viking Graben, *Geology,* **20,** 47–50.

McClusky, S. *et al.*, 2000. Global Positioning System constraints on plate kinematics and dynamics in the eastern Mediterranean and Caucasus, *J. geophys. Res.,* **105,** 5695–5719.

McKenzie, D., 1972. Active tectonics of the Mediterranean region, *Geophys. J. R. astr. Soc.,* **30,** 109–185.

McKenzie, D., 1978. Active tectonics of the Alpine-Himalayan belt: the Aegean Sea and surrounding regions, *Geophys. J. R. astr. Soc.,* **55,** 217–254.

Melis, N.S., Burton, P.W. & Brooks, M., 1995. Coseismic crustal deformation from microseismicity in the Patras area, western Greece, *Geophys. J. Int.,* **122,** 815–836.

Michael, A.J., 1987. Use of focal mechanisms to determine stress: a control study, *J. geophys. Res.,* **92,** 357–368.

Muço, B., 1994. Focal mechanism solutions for Albanian earthquakes for the years 1964–1988, *Tectonophysics,* **231,** 311–323.

Nicolas, M., Santoire, J.P. & Delpech, P.Y., 1990. Intraplate seismicity: new seismotectonic data in western Europe, *Tectonophysics,* **179,** 27–53.

Ouyed, M., Yielding, G., Hatzfeld, D. & King, G.C.P., 1983. An aftershock study of the El Asnam (Algeria) earthquake of 1980, October 10, *Geophys. J. R. astr. Soc.,* **73,** 605–639.

Panagiotopoulos, D., Papadimitriou, E., Papaioannou, C., Scordilis, E. & Papazachos, B.C., 1993. Source properties of the December 21, 1990, Goumenissa earthquake in Northern Greece, *Proc. 2nd Congr. Hell. Geophys. Un.*, pp. 275–285, Florina, Greece.

Papadimitriou, E.E., 1992. Focal mechanisms along the convex side of the Hellenic Arc and its tectonic significance, *Publ. Geophys. Lab. University Thessaloniki,* **8,** 1–20.

Papadimitriou, E.E., 1993. Focal mechanism along the convex side of the Hellenic Arc, *Boll. Geofis. Teor. Appl.,* **35,** 401–426.

Papazachos, B., Panagiotopoulos, D., Tsapanos, Th., Mountrakis, D. & Dimopoulos, G., 1983. A study of the 1980 summer seismic sequence in the Magnesia region of central Greece, *Geophys. J. R. astr. Soc.,* **75,** 155–168.

Papazachos, B., Kiratzi, A., Voidomatis, Ph. & Papaioannou, Ch., 1984. A study of the December, 1981–January, 1982 seismic activity in northern Aegean Sea, *Boll. Geofis. Teor. Appl.,* **26,** 101–102.

Papazachos, B., Kiratzi, A., Karacostas, B., Panagiotopoulos, D., Scordilis, E. & Mountrakis, D., 1988. Surface fault traces, fault plane solutions and spatial distribution of the aftershocks of the September 13, 1986 earthquake of Kalamata (southern Greece), *Pure appl. Geophys.,* **126,** 55–68.

Papazachos, B.C. & Delibasis, N.D., 1969. Tectonic stress field and seismic faulting in the area of Greece, *Tectonophysics,* **7,** 231–255.

Papazachos, B.C., Kiratzi, A.A. & Papadimitriou, E., 1991. Fault plane solutions for earthquakes in the Aegean area, *Pure appl. Geophys.,* **136,** 405–420.

Papazachos, B.C., Kiratzi, A.A. & Papazachos, B., 1992. Rates of active crustal deformation in the Aegean and the surrounding area, *J. Geodyn.,* **16,** 147–179.

Papazachos, B.C., Papadimitriou, E.E., Kiratzi, A.A., Papazachos, C.B. & Louvari, K., 1998. Fault plane solutions in the Aegean Sea and the surrounding area and their tectonic implication, *Boll. Geofis. Teor. Appl.,* **39,** 199–218.

Papazachos, C.B. & Kiratzi, A.A., 1992. A formulation for reliable estimation of active crustal deformation and its application to central Greece, *Geophys. J. Int.,* **111,** 424–432.

Papazachos, C.B. & Kiratzi, A., 1996. A detailed study of the active crustal deformation in the Aegean and surrounding area, *Tectonophysics,* **253,** 129–153.

Polimenos, G., 2000. Scaling properties of normal fault populations in the western Corinth Graben, Greece: implications for fault growth in large strain settings, *J. struct. Geol.,* **22,** 307–322.

Pondrelli, S., 1999. Pattern of seismic deformation in the western Mediterranean, *Ann. Geofis.,* **42,** 57–70.

Pondrelli, S., Morelli, A. & Boschi, E., 1995. Seismic deformation in the Mediterranean area estimated by moment tensor summation, *Geophys J. Int.,* **122,** 938–952.

Press, W.H., Flannery, B.P., Teukolsky, S.A. & Vetterling, W.T., 1986. *Numerical Recipes. The Art of Scientific Computing,* Cambridge University Press, Cambridge.

Priestley, K., Baker, C. & Jackson, J., 1994. Implications of earthquake focal mechanism data for the active tectonics of the south Caspian Basin and surrounding regions, *Geophys. J. Int.,* **118,** 111–141.

Reilinger, R. *et al.*, 1997. GPS measurements of present-day crustal movements in the Arabia-Africa-Eurasia Plate collision zone, *J. geophys. Res.,* **102,** 9983–9999.

Renner, G. & Slejko, D., 1994a. Sismicità strumentale della regione Adriatica, *Proc. 13th GNGTS Meeting,* pp. 907–913, Roma, Italy.

Renner, G. & Slejko, D., 1994b. Some comments on the seismicity of the Adriatic region, *Boll. Geof. Teor. Appl.,* **36,** 381–398.

Renner, G., Poli, M.E. & Slejko, D., 1991. Il terremoto dell'11 Giugno 1991 nelle prealpi carniche orientali, *Proc. 10th GNGTS Meeting,* pp. 305–316, Roma, Italy.

Ribeiro, A., Cabral, J., Baptista, R. & Matias, L., 1996. Stress pattern in Portugal mainland and the adjacent Atlantic region, West Iberia, *Tectonics,* **15,** 641–659.

Rigo, A., Lyon-Caen, H., Armijo, R., Deschamps, A., Hatzfeldt, D., Makropoulos, K., Papadimitriou, P. & Kassaras, I., 1996. A microseismic study in the western part of the Gulf of Corinth (Greece): implications for large-scale normal faulting mechanisms, *Geophys. J. Int.,* **126,** 663–688.

Ritsema, A.R., 1974. *The Earthquake Mechanisms of the Balkan Region,* R. Neth. Meteorol. Inst. De Bilt, Rept 74.

Rocca, A., Karakaisis, G., Karacostas, B., Kiratzi, A., Scordilis, E. & Papazachos, B., 1985. Further evidence on the strike-slip faulting of the northern Aegean trough based on properties of the August–November, 1983 seismic sequence, *Boll. Geof. Teor. Appl.,* **27,** 101–109.

Scordilis, E., Karakaisis, G., Karacostas, B., Panagiotopoulos, D., Comninakis, P. & Papazachos, B., 1985. Evidence for transform faulting in the Ionian Sea: the Cephalonia island earthquake sequence of 1983, *Pageoph,* **123,** 388–397.

Shen-Tu, B., Holt, W.E. & Haines, A.J., 1995. Intraplate deformation in the Japanese Islands: a kinematic study of intraplate deformation at a convergent plate margin, *J. geophys. Res.,* **100,** 24 275–24 293.

Shen-Tu, B., Holt, W.E. & Haines, A.J., 1998. Contemporary kinematics of the western United States determined from earthquake moment tensors, very long baseline interferometry, and GPS observations, *J. geophys. Res.,* **103,** 18 087–18 117.

Shirokova, E., 1972. Stress pattern and probable motion in the earthquake foci of the Asia-Mediterranean seismic belt, in *Elastic Strain Field of the Earth and Mechanics of Earthquake Sources,* ed. Balakina, L.M., Nauka, Moscow.

Simpson, R., 1997. Quantifying Anderson's fault types, *J. geophys. Res.,* **102,** 17 909–17 919.

Sipkin, S.A. & Needham, R.E., 1991. Moment-tensor solutions estimated using optimal filter theory: global seismicity, 1988–1989, *Phys. Earth planet. Inter.,* **67,** 221–230.

Slejko, D. *et al.*, 1989. Seismotectonics of the eastern-southern Alps: a rewiew, *Boll. Geofis. Teor. Appl.,* **31,** 109–136.

Sobouti, F. & Arkani-Hamed, J., 1996. Numerical modelling of the deformation of the Iranian plateau, *Geophys. J. Int.,* **126,** 805–818.

Soufleris, Ch. & Stewart, G., 1981. A source study of the Thessaloniki (N. Greece) 1978 earthquake sequence, *Geophys. J. R. astr. Soc.,* **67,** 343–358.

Suleiman, A.S. & Doser, D.I., 1995. The seismicity, seismotectonics and earthquake hazards of Lybia, with detailed analysis of the 1935 April 19, $M = 7.1$ earthquake sequence, *Geophys. J. Int.,* **120,** 312–322.

Taymaz, T., 1993. The source parameters of the Cubukdag (W. Turkey) earthquake of 1986 October 11, *Geophys. J. Int.,* **113,** 260–267.

Taymaz, T. & Price, S., 1992. The 1971, May 12 Burdur earthquake sequence, SW Turkey: a synthesis of seismological and geological observations, *Geophys. J. Int.,* **108,** 589–603.

Taymaz, T., Jackson, J. & Westaway, R., 1990. Earthquake mechanisms in the Hellenic Trench near Crete, *Geophys. J. Int.,* **102,** 695–731.

Taymaz, T., Jackson, J. & McKenzie, D., 1991a. Active tectonics of the north and central Aegean Sea, *Geophys. J. Int.,* **106,** 433–490.

Taymaz, T., Eyidogan, H. & Jackson, J., 1991b. Source parameters of large earthquakes in the East Anatolian Fault Zone (Turkey), *Geophys. J. Int.,* **106,** 537–550.

Thouvenot, F., *et al.*, 1998. The M_L 5.3 Epagny (French Alps) earthquake of 1996, July 15: a long-awaited event on the Vauche Fault, *Geophys. J. Int.,* **135,** 876–892.

Twiss, R.J. & Unruh, J.R., 1998. Analysis of fault slip inversions: do they constrain stress or strain rate?, *J. geophys. Res.,* **103,** 12 205–12 222.

Udias, A., Buforn, E. & Ruiz de Gauna, J., 1989. *Catalogue of Focal Mechanisms of European Earthquakes,* Universidad Complutense, Madrid.

Wang, J.-H. & Ou, S.-S., 1998. On scaling of earthquake faults, *Bull. seism. Soc. Am.,* **88,** 758–766.

Ward, S.N., 1998. On the consistency of earthquake moment release and space geodetic strain rates: Europe, *Geophys. J. Int.,* **135,** 1011–1018.

Wessel, P. & Smith, H.F., 1995. New version of the Generic Mapping Tool released, *EOS, Trans. Am. geophys. Un.,* **76,** 329.

Westaway, R., 1987. The Campania, southern Italy, earthquakes of 1962, August 21, *Geophys. J. R. astr. Soc.,* **88,** 1–24.

Westaway, R., 1990. Block rotation in western Turkey, *J. geophys. Res.,* **95,** 19 857–19 884.

Westaway, R. & Jackson, J., 1987. The earthquake of 1980 November 23 in Campania–Basilicata (southern Italy), *Geophys. J. Int.,* **90,** 375–443.

Wyss, M., Liang, B., Tanigawa, W.R. & Wu, X., 1992. Comparison of orientations of stress and strain tensors based on fault plane solutions in Kaoiki, Hawaii, *J. geophys. Res.,* **97,** 4769–4790.

Zanchi, A. & Angelier, J., 1993. Seismotectonics of western Anatolia, regional stress orientation from geophysical and geological data, *Tectonophysics,* **222,** 259–274.

APPENDIX A: DESCRIPTION OF THE DATA SET

Source parameters of the 2029 earthquakes used in the present study, which occurred in the period September 1905–March 1999 within the area 24°N – 53°N, 30°W – 60°E, are currently available as a digital ASCII file (FM-APPENDIX1.TXT) on the anonymous ftp site ibogfs.df.unibo.it/albarello. Each record contains one fault plane solution. The tab character separates pieces of information distributed over 20 numerical and alphanumerical fields whose contents are described below.

Fields 1 – 3: event date (year, month, day, respectively).

Fields 4 – 6: GMT origin time (hour, minute, second, respectively).

Fields 7 – 8: epicentral coordinates (north latitude and east longitude, respectively, in degrees).

Field 9: hypocentral depth (km); the value zero indicates events classified as 'shallow'.

Fields 10 – 11: magnitude classifier and magnitude. Values 0, 1 and 2 in field 10 indicate that either no or M_S or m_b magnitude, respectively, is reported in field 11.

Field 12: seismic moment M_0 (scale factor 10^{16} N m); the value zero indicates that no estimate of M_0 is reported in the relevant source.

Fields 13 – 15: strike, dip, rake (degree) of one nodal plane of the focal mechanism. Angles refers to the convention described by Jost & Herrmann (1989).

Fields 16 – 17: trend and plunge (degree) of the T-axis.

Fields 18 – 19: trend and plunge (degree) of the P-axis.

Field 20: code referring to the reference from which the datum has been taken. The list of references of focal mechanisms is given in the file SO-APPENDIX1.TXT available on the same ftp site (Amoruso *et al.* 1998; Anderson & Jackson 1987; Baker *et al.* 1993, 1997; Bernard *et al.* 1997; Bonjer 1997; Boore *et al.* 1981; Buforn *et al.* 1988; Cipar 1981; Deschamps & King 1984; Dziewonski *et al.* 1983; Ekström & England 1989; Ekström & Nettles 1997; Eva & Pastore 1993; Eva *et al.* 1988, 1997; Eyidogan 1988; Eyidogan & Jackson 1985; Frepoli & Amato 1997; Gallart *et al.* 1985; Gasparini *et al.* 1985; Giardini *et al.* 1985; Grimison & Chen 1988; Grunthal & Stromeyer 1992; Hatzfeld *et al.* 1993; Jackson & McKenzie 1988; Jackson *et al.* 1992; Karakaisis *et al.* 1993; Kiratzi 1999; Kiratzi & Langston 1989; Kiratzi *et al.* 1991; Larson 1999; Liotier 1989; Lyon-Caen *et al.* 1988; McKenzie 1972, 1978; Melis *et al.* 1995; Muço 1994; Nicolas *et al.* 1990; Ouyed *et al.* 1983; Panagiotopoulos *et al.* 1993; Papadimitriou 1992, 1993; Papazachos & Delibasis 1969; Papazachos *et al.* 1983, 1984, 1988, 1991; Priestley *et al.* 1994; Renner & Slejko 1994a,b; Renner *et al.* 1991; Ribeiro *et al.* 1996; Rigo *et al.* 1996; Ritsema 1974; Rocca *et al.* 1985; Scordilis *et al.* 1985; Shirokova 1972; Sipkin & Needham 1991; Slejko *et al.* 1989; Soufleris & Stewart 1981; Suleiman & Doser 1995; Taymaz 1993; Taymaz & Price 1992; Taymaz *et al.* 1990, 1991a,b; Thouvenot *et al.* 1998; Udias *et al.* 1989; Westaway 1987, 1990; Westaway & Jackson 1987; Zanchi & Angelier 1993).